Solar Physics (2006) 233: 215–232
DOI: 10.1007/s11207-006-2092-z

PREPROCESSING OF VECTOR MAGNETOGRAPH DATA FOR A NONLINEAR FORCE-FREE MAGNETIC FIELD RECONSTRUCTION

T. WIEGELMANN and B. INHESTER
Max-Planck-Institut für Sonnensystemforschung, Katlenburg-Lindau, Germany
(e-mail: wiegelmann@linmpi.mpg.de)

and

T. SAKURAI
National Astronomical Observatory of Japan, Solar Physics Division, Mitaka, Tokyo, Japan

(Received 10 May 2005; accepted 15 July 2005)

Abstract. Knowledge regarding the coronal magnetic field is important for the understanding of many phenomena, like flares and coronal mass ejections. Because of the low plasma beta in the solar corona, the coronal magnetic field is often assumed to be force-free and we use photospheric vector magnetograph data to extrapolate the magnetic field into the corona with the help of a non-linear force-free optimization code. Unfortunately, the measurements of the photospheric magnetic field contain inconsistencies and noise. In particular, the transversal components (say B_x and B_y) of current vector magnetographs have their uncertainties. Furthermore, the magnetic field in the photosphere is not necessarily force free and often not consistent with the assumption of a force-free field above the magnetogram. We develop a preprocessing procedure to drive the observed non–force-free data towards suitable boundary conditions for a force-free extrapolation. As a result, we get a data set which is as close as possible to the measured data and consistent with the force-free assumption.

1. Introduction

The structure of the solar corona out to a few solar radii is dominated by the magnetic field. Knowledge regarding the coronal magnetic field is therefore important to understand physical processes like flares and coronal mass ejections. Unfortunately, direct measurements of the magnetic field are difficult for the following reasons: the high plasma temperature in the corona broadens the line profile orders of magnitudes above the Zeeman splitting. In addition, coronal lines are optical thin and consequently the line-of-sight integrated character of the measurements complicates their interpretation.

It has been proposed to use magnetic sensitive coronal line observations in order to constrain the coronal magnetic field (see, *e.g.*, House, 1977; Arnaud and Newkirk, 1987; Judge, 1998). Lin, Kuhn, and Coulter (2004) demonstrated that Zeeman-effect measurements can be performed. However, due to the line-of-sight effect, the interpretation of these lines is difficult. Also, recent measurements of chromospheric and lower coronal magnetic fields were made for a few individual

cases, *e.g.* (Solanki *et al.*, 2003) and (Lagg *et al.*, 2004). Such multi-wavelength spectropolarimetric observations have not been done routinely in the past but are believed to become much more commonplace, and reliable, in the near future.

As an alternative to these direct measurements, methods have been developed to use the magnetic field observed on the photosphere for an extrapolation into the corona. The extrapolation is not free from assumptions regarding the coronal plasma. It is helpful, that the low and middle corona contains a low-β plasma, which allows the neglect of the plasma pressure in first order, and use of a force-free magnetic field model. A force-free magnetic field is characterized by the electric currents parallel to the magnetic field lines, *i.e.*,

$$\nabla \times \mathbf{B} = \alpha \mathbf{B} \tag{1}$$

$$\nabla \cdot \mathbf{B} = 0 \tag{2}$$

where the coefficient α is constant along the field lines but may vary between different field lines. Since (1), due to its intrinsic nonlinearity, is difficult to solve, simplifications of (1) are sometimes used like potential fields ($\alpha = 0$, i.e., no currents; see *e.g.* Schmidt, 1964; Semel, 1967; Cuperman, Ofman, and Semel, 1989) and linear force-free fields ($\alpha =$ constant; see *e.g.* Chiu and Hilton, 1977; Seehafer, 1978, 1982; Alissandrakis, 1981; Semel, 1988; Demoulin and Priest, 1992).

The nonlinear force-free case (Sakurai, 1981; Wu *et al.*, 1990; Roumeliotis, 1996; Amari *et al.*, 1997; Yan and Sakurai, 2000; Wheatland, Sturrock, and Roumeliotis, 2000; Wheatland, 2004; Régnier, Amari, and Kersalé, 2002; Wiegelmann and Neukirch, 2003; Wiegelmann, 2004; Valori, Kliem, and Keppens, 2005) is challenging both theoretically due to the nonlinearity of the underlying mathematical problem and observationally because a measurement of the full magnetic vector on the photospheric is required. For investigations of instabilities like filament eruptions, it is essential to consider the general nonlinear force-free field case because the free magnetic energy that might drive the instability cannot be described with the simplified field models mentioned earlier.

Moreover, a comparison between extrapolations and measured fields (Solanki *et al.*, 2003) in a newly developed active region revealed that a nonlinear model agrees better with the observations than a potential and linear force-free magnetic field model (Wiegelmann *et al.*, 2005).

A nonlinear force-free extrapolation of coronal magnetic fields from measured photospheric data is a challenging problem for several reasons. The magnetic field in the photosphere is not necessarily force-free (see Gary, 2001), and one would rather prefer to use the vector-magnetic field at the basic of the corona as boundary condition for a nonlinear force-free extrapolation, but here measurements are usually not available.

Another problem is the 180° ambiguity in the transverse components of the photospheric data, which has to be removed with *e.g.* the minimum energy method (Metcalf, 1994). An additional complication is that the transverse components

are more difficult to measure and have much more noise than the line-of-sight component. For the data of the Solar-Flare Telescope (SFT) used in Section 5, for example, the noise level is about 10 G for the line-of-sight magnetic field and 100 G for the transverse field. The full-disk vector magnetograph SOLIS (Synoptic Optical Long-term Investigations of the Sun, U.S. National Solar Observatory, Kitt Peak) is expected to have a noise level of about 1 G in the line-of-sight and about 50 G in the transverse components (C. Keller, private communication). The reason for the much higher noise in the transverse magnetic field (B_t) compared with the line-of-sight field (B_L) can be understood by the way in which the photospheric magnetic field is derived from the four measured Stokes components. Roughly $B_\mathrm{L} = c_1 V/I$, where V is the circular polarization and c_1 is a constant. Then

$$\delta B_\mathrm{L} = c_1 \frac{\delta V}{I} \sim \frac{\delta I}{I} \sim \sqrt{I}, \tag{3}$$

where δI is the noise in I. This photon noise is independent of B_L. Even if the Q and U signals are generally weaker than the V signal, the major source of errors in the force balance is the noise in B_t: $B_\mathrm{t}^2 = c_2 \sqrt{Q^2 + U^2}/I$ where Q and U are linear polarization intensities and c_2 is another constant. Then

$$2B_\mathrm{t}\,\delta B_\mathrm{t} = c_2 \frac{Q\delta Q + U\delta U}{\sqrt{Q^2 + U^2} I} \sim c_2 \frac{\sqrt{\delta Q^2 + \delta U^2}}{I} \sim c_2 \frac{\delta I}{I} \sim \text{constant}. \tag{4}$$

As a consequence, the transverse magnetic field noise is in particular high in weak field regions. In strong-field regions, vector magnetic field measurements based on full Stokes spectro-polarimetry generally yield uncertainties of a few degrees in the orientation angles of the field vector in active regions. This situation is also constantly improving with improved instrumentation.

For the practical computation of the coronal magnetic field, it is also helpful if the boundary data are smoothed to some degree. Short wavelength fluctuations in the surface magnetic field die out rapidly with height (for a potential field with $\exp(-kz)$ for scales of horizontal wavenumber k). Hence, boundary data with scales much finer than the height of the numerical box require a very fine grid to be sufficiently resolved but they hardly have an effect on the result, except in a very small boundary layer above the surface. To keep the numerical effort limited, the boundary data are therefore usually smoothed. In this context it should also be noted that the force-free equation (1) is scale invariant if α is rescaled appropriately. Hence, by smoothing of the boundary data we do not lose any physics which we have not already cast away by the restriction to a stationary force-free field model.

A more fundamental requirement on the boundary data is its consistency with the force-free field approximation. As has been shown by Aly (1989), a balance of the total momentum and angular momentum exerted onto the numerical box by the magnetic field leads to a set of boundary integral constraints for the magnetic field. These constraints should also be satisfied on the solar surface for the field at

the coronal base in the vicinity of a sufficiently isolated magnetic region and in a situation where there is no rapid dynamical development.

In summary, the boundary data for the force-free extrapolation should fulfill the following conditions:

1. The data should coincide with the photospheric observations within measurement errors.
2. The data should be consistent with the assumption of a force-free magnetic field mentioned earlier.
3. For computational reasons (finite differences), the data should be sufficiently smooth.

Within this work we describe a numerical procedure, written in IDL, which preprocesses vector magnetograph data so that the aforementioned conditions are satisfied as close as possible.

We outline the paper as follows. In Section 2 we specify how to check if a given measured vector magnetograms is consistent with the assumption of a force-free magnetic field in the corona above the magnetogram. We describe how to derive consistent force-free boundary conditions for a force-free magnetic field extrapolation from the measured data in Section 3. In Section 4 we use a known semi-analytic force-free model to check our method and we apply the method in Section 5 to an example of the observed vector magnetogram.

2. Consistency Check of Vector Magnetograms

In the following we assume that the 180° ambiguity in the measured transverse components has been removed and the magnetogram has been observed close to the disk center. "Close" here means that the vertical component B_z in our numerical box can be more or less identified with the line-of-sight component and bears a smaller measurement error than the horizontal components B_x and B_y. Since, as stated earlier, the measurement error between the line-of-sight and the transverse components differs by about one order of magnitude, the angle between line-of-sight and vertical should not exceed $\simeq 0.1$ rad.

Another *a-priori* assumption about the photospheric data is that the magnetic flux from the photosphere is sufficiently distant from the boundaries of the observational domain and the net flux is in balance, *i.e.*,

$$\int_S B_z(x, y, 0)\, \mathrm{d}x\, \mathrm{d}y = 0. \tag{5}$$

Generally, the flux balance criterion has to be applied to the whole, closed surface of the numerical box. However, we can only measure the magnetic field vector on the bottom photospheric boundary and the contributions of the lateral and top boundary remain unspecified. However, if a major part of the known flux from the

bottom boundary is uncompensated, the final force-free magnetic field solution will markedly depend on how the uncompensated flux is distributed over the other five boundaries. This would result in a major uncertainty of the final force-free magnetic field configuration. We therefore demand the flux balance to be satisfied with the bottom data alone. If this is not the case, we classify the reconstruction problem as not uniquely solvable within the given box.

Aly (1989) used the virial theorem to define which conditions a vector magnetogram has to fulfill to be consistent with the assumption of a force-free field mentioned earlier. We repeat here the force-free and torque-free condition and refer to the paper of (Aly, 1989) for details.

1. The total force on the boundary vanishes

$$\int_S B_x B_z \, \mathrm{d}x \, \mathrm{d}y = \int_S B_y B_z \, \mathrm{d}x \, \mathrm{d}y = 0$$

$$\int_S (B_x^2 + B_y^2) \, \mathrm{d}x \, \mathrm{d}y = \int_S B_z^2 \, \mathrm{d}x \, \mathrm{d}y.$$

2. The total torque on the boundary vanishes

$$\int_S x \, \left(B_x^2 + B_y^2\right) \, \mathrm{d}x \, \mathrm{d}y = \int_S x \, B_z^2 \, \mathrm{d}x \, \mathrm{d}y$$

$$\int_S y \, \left(B_x^2 + B_y^2\right) \, \mathrm{d}x \, \mathrm{d}y = \int_S y \, B_z^2 \, \mathrm{d}x \, \mathrm{d}y$$

$$\int_S y \, B_x B_z \, \mathrm{d}x \, \mathrm{d}y = \int_S x \, B_y B_z \, \mathrm{d}x \, \mathrm{d}y$$

Note that if condition (1) is fulfilled, the constraints (2) are independent of where the origin for x, y is located. In our code, the origin is usually at the lower left corner of the bottom boundary face.

As with the flux balance, the Aly integral criteria in general have to be applied to the whole surface of the numerical box. Since we assumed that the photospheric flux is sufficiently concentrated in the center and the net flux is in balance, we can expect the magnetic field on the lateral and top boundary to remain small and hence these surfaces will not yield a large contribution to the integrals of the Aly constraints mentioned earlier. We therefore impose the Aly criteria on the bottom boundary alone.

Aly (1989) already pointed out that the magnetic field is probably not force-free in the measured region because the plasma β in the photosphere is of the order of one and pressure and gravity forces are not negligible. We however expect that the observed photospheric field is, after removing scales below a super-granular diameter by smoothing, representative of the field at the coronal base. In the corona, however, we have $\beta \approx 10^{-4}$, and consequently the magnetic field should be close to force-free in a stationary situation.

To quantify the quality of vector magnetograms with respect to the aforementioned criteria, we introduce three dimensionless parameters:

1. The flux balance parameter

$$\epsilon_{\text{flux}} = \frac{\int_S B_z \, \mathrm{d}x \, \mathrm{d}y}{\int_S |B_z| \, \mathrm{d}x \, \mathrm{d}y}$$

2. The force balance parameter

$$\epsilon_{\text{force}} = \frac{\left| \int_S B_x B_z \, \mathrm{d}x \, \mathrm{d}y \right| + \left| \int_S B_y B_z \, \mathrm{d}x \, \mathrm{d}y \right| + \left| \int_S \left(B_x^2 + B_y^2\right) - B_z^2 \, \mathrm{d}x \, \mathrm{d}y \right|}{\int_S \left(B_x^2 + B_y^2 + B_z^2\right) \mathrm{d}x \, \mathrm{d}y}$$

3. The torque balance parameter

$$\epsilon_{\text{torque}} = \frac{\left| \int_S x\left(\left(B_x^2+B_y^2\right) - B_z^2\right)\mathrm{d}x\mathrm{d}y \right| + \left| \int_S y\left(\left(B_x^2+B_y^2\right) - B_z^2\right)\mathrm{d}x \, \mathrm{d}y \right| + \left| \int_S y B_x B_z - x B_y B_z \mathrm{d}x\mathrm{d}y \right|}{\int_S \sqrt{x^2+y^2}\left(B_x^2 + B_y^2 + B_z^2\right)\mathrm{d}x \, \mathrm{d}y}$$

An observed vector magnetogram is then flux-balanced and consistent with the force-free assumption if: $\epsilon_{\text{flux}} \ll 1$, $\epsilon_{\text{force}} \ll 1$, $\epsilon_{\text{torque}} \ll 1$.

3. Method

Even if we choose a sufficiently flux-balanced isolated active region ($\epsilon_{\text{flux}} \ll 1$) we find that usually the force-free conditions ($\epsilon_{\text{force}} \ll 1$, $\epsilon_{\text{torque}} \ll 1$) are not fulfilled for measured vector magnetograms. We conclude, therefore, that nonlinear force-free extrapolation methods may not be used directly on observed vector magnetograms, in particular not on the very noisy transverse photospheric magnetic field measurements. The large noise in the transverse components of the photospheric field vector ($\sim$ the horizontal B_x and B_y at the bottom boundary) gives us the freedom to adjust these data within the noise level. We use this freedom to drive the data towards being more consistent with Aly's force-free and torque-free conditions.

As a measure of how well a photospheric magnetic field agrees with Aly's criteria, the observed data, and the smoothness condition, we define the following functional which adds up the χ^2 deviations from all of the individual constraints:

$$L = \mu_1 L_1 + \mu_2 L_2 + \mu_3 L_3 + \mu_4 L_4 \tag{6}$$

where

$$L_1 = \left[\left(\sum_p B_x B_z \right)^2 + \left(\sum_p B_y B_z \right)^2 + \left(\sum_p B_z^2 - B_x^2 - B_y^2 \right)^2 \right]$$

$$L_2 = \left[\left(\sum_p x\left(B_z^2 - B_x^2 - B_y^2\right) \right)^2 + \left(\sum_p y\left(B_z^2 - B_x^2 - B_y^2\right) \right)^2 + \left(\sum_p y B_x B_z - x B_y B_z \right)^2 \right]$$

$$L_3 = \left[\sum_p (B_x - B_{x\mathrm{obs}})^2 + \sum_p (B_y - B_{y\mathrm{obs}})^2 + \sum_p (B_z - B_{z\mathrm{obs}})^2 \right]$$

$$L_4 = \left[\sum_p (\Delta B_x)^2 + (\Delta B_y)^2 + (\Delta B_z)^2 \right] \tag{7}$$

The surface integrals are here replaced by a summation $\sum_p$ over all p grid nodes of the bottom surface grid, and the differentiation in the smoothing term is achieved by the usual five-point stencil for the 2D-Laplace operator. Each constraint L_n is weighted by a yet undetermined factor μ_n. The first term ($n = 1$) corresponds to the force-balance condition, the next ($n = 2$) to the torque-free condition. The following term ($n = 3$) ensures that the optimized boundary condition agrees with the measured photospheric data, and the last terms ($n = 4$) controls the smoothing. The 2D-Laplace operator is designated by Δ.

The aim of our preprocessing procedure is to minimize L so that all terms L_n, if possible, are made small simultaneously. This will yield a surface magnetic field

$$\mathbf{B}_{\min} = \mathrm{argmin}(L) \tag{8}$$

Besides a dependence on the observed magnetogram, the solution (8) now also depends on the coefficients μ_n. These coefficients are a formal necessity because the terms L_n represent different quantities with different units. By means of these coefficients, however, we can also give more or less weight to the individual terms in the case where a reduction in one term apposes the reduction in another. This competition obviously exists between the observation term ($n = 3$) and the smoothing term ($n = 4$).

The smoothing is performed consistently for all three magnetic field components. For this purpose we need the derivative of L with respect to each of the three field components at every node (q) of the bottom boundary grid. We have, however, taken account of the fact that B_z is measured with much higher accuracy than B_x and B_y. This is achieved by assuming the vertical component invariable compared to the horizontal components in all terms where mixed products of the vertical and horizontal field components occur, *e.g.*, in the Aly constraints. The relevant functional derivative of L is therefore

$$\frac{\mathrm{d}L}{\mathrm{d}(B_x)_q} = 2\mu_1 \left[\left(\sum_p B_x B_z \right)(B_z)_q - 2\left(\sum_p B_x^2 \right)(B_x)_q \right]$$

$$
\begin{aligned}
&- 2\mu_2\left[2\left(\sum_p x\left(B_z^2 - B_x^2 - B_y^2\right)\right)(xB_x)_q\right.\\
&+ 2\left(\sum_p y\left(B_z^2 - B_x^2 - B_y^2\right)\right)(yB_x)_q\\
&\left.-\left(\sum_p yB_xB_z - xB_yB_z\right)(yB_z)_q\right]\\
&+ 2\mu_3(B_x - B_{x\mathrm{obs}})_q + 2\mu_4(\Delta(\Delta B_x))_q \qquad (9)
\end{aligned}
$$

$$
\begin{aligned}
\frac{\mathrm{d}L}{\mathrm{d}(B_y)_q} &= 2\mu_1\left[\left(\sum_p B_yB_z\right)(B_z)_q - 2\left(\sum_p B_y^2\right)(B_y)_q\right]\\
&- 2\mu_2\left[2\left(\sum_p x\left(B_z^2 - B_x^2 - B_y^2\right)\right)(xB_y)_q\right.\\
&+ 2\left(\sum_p y\left(B_z^2 - B_x^2 - B_y^2\right)\right)(yB_y)_q\\
&\left.+\left(\sum_p yB_xB_z - xB_yB_z\right)(xB_z)_q\right]\\
&+ 2\mu_3(B_y - B_{y\mathrm{obs}})_q + 2\mu_4(\Delta(\Delta B_y))_q \qquad (10)
\end{aligned}
$$

$$
\frac{\mathrm{d}L}{\mathrm{d}(B_z)_q} = 2\mu_3(B_z - B_{z\mathrm{obs}})_q + 2\mu_4(\Delta(\Delta B_z))_q \qquad (11)
$$

The optimization is performed iteratively by a simple Newton scheme which replaces

$$
\begin{aligned}
(B_x)_q &\leftarrow (B_x)_q - \mu\frac{\mathrm{d}L}{\mathrm{d}(B_x)_q}\\
(B_y)_q &\leftarrow (B_y)_q - \mu\frac{\mathrm{d}L}{\mathrm{d}(B_y)_q} \qquad (12)\\
(B_z)_q &\leftarrow (B_z)_q - \mu\frac{\mathrm{d}L}{\mathrm{d}(B_z)_q} \qquad (13)
\end{aligned}
$$

at every step. The convergence of this scheme towards a solution of (8) is obvious: L has to decrease monotonically at every step as long as (9) – (11) has a nonzero component. These terms, however, vanish only if an extremum of L is reached. Since L is fourth order in B, this may not necessarily be a global minimum, in rare cases if the step size is handled carelessly it may even be a local maximum. In practical

calculations this should, however, not be a problem and from our experience we rapidly obtain a minimum $\mathbf{B}_{\min}$ of L, once the parameters μ_n are specified.

What is left is a suitable recipe to choose μ_n. We have four parameters (μ_n) to choose and we restrict our freedom a little bit by giving the same weight $\mu_1 = \mu_2 D^2 \equiv \mu_{12}$ to the Aly momentum and torque constraints where D is the edge length of our numerical square box. Accordingly, we will combine $L_1 + L_2/D^2 \equiv L_{12}$. We are then left with three parameters, only two of which are independent since only the ratio of the parameters really counts. Multiplying all μ_n by a common factor does not change the minimum-solution B of the preprocessed photospheric data. We use this fact and specify μ_{12} to be $1/B_{\text{ave}}^2$ where B_{ave} is the average magnetic field magnitude in our magnetogram.[1]

With the parameters μ_3 and μ_4 we can now control the relative influence of the observed data and the smoothing, with respect to one another, and with respect to the Aly constraints. For the proper selection of these parameters, we proceed in a similar way as is customary for regularization techniques of inversion problems (*e.g.* Hansen, 2001). For this purpose, we visualize the different solutions $\mathbf{B}_{\min}(\mu_3, \mu_4)$ for different μ parameters in a phase space of $\log(L_{12})$, $\log(L_3)$, and $\log(L_4)$. Since the L-terms depend analytically on $\mathbf{B}$, the solutions $\mathbf{B}_{\min}$ span a continuous 2D surface in this 3D phase space.

A survey of the μ parameters for one of the example computations (Low and Lou solution with noise model I) described in the next section shows that $\log(L_3(\mathbf{B}_{\min}))$ and $\log(L_4(\mathbf{B}_{\min}))$ are almost entirely determined by the ratio of μ_3 to μ_4, while $\log(L_{12}(\mathbf{B}_{\min}))$ depends on the absolute magnitude of μ_3 and μ_4. It is therefore convenient to display our results in a projection of the 3D phase space along the $\log(L_{12})$-axis as in Figure 1. In this projection, the surface collapses nearly to a unique curve.

An obvious limiting value is obtained for $\mu_3 \to \infty$ which yields $\mathbf{B}_{\min} = \mathbf{B}_{\text{obs}}$ with $L_{12} \sim 10^{-1}$, $L_3 = 0$, and $L_4 \sim 10^{-3}$. For smaller values of μ_3 we obtain a smoothed solution and, depending on μ_4, also satisfy the Aly criteria much better than the original observational data. The price we have to pay is that L_3 attains finite values, which however is tolerable as long as L_3 does not exceed a noise value $L_3(\mathbf{B}_{\text{noise}})$ (dotted line in Figure 1). This value in our test case is known from the amount of noise added. For actual observations, it has to be estimated. The intersection of our solution surface with the noise level then defines the optimal ratio of μ_3 to μ_4 (marked by a rhombus in Figure 1). We choose both numbers to be small to enforce a good compliance with the Aly criteria, *i.e.*, give great weight to L_{12}. This way, L_{12} is reduced by 6 orders of magnitude, B is conveniently smoothed and yet it does not deviate from the observations by more than the instrumental error. The smoothing will somewhat broaden prominent magnetic flux structures. A careful choice of the preprocessing parameters (as described earlier) ensures

[1]Note that this is equivalent to a normalization of the magnetic field with B_{ave} and the length scale with D. With this normalization we get $L_1 = L_2 = L_{12} = 1$.

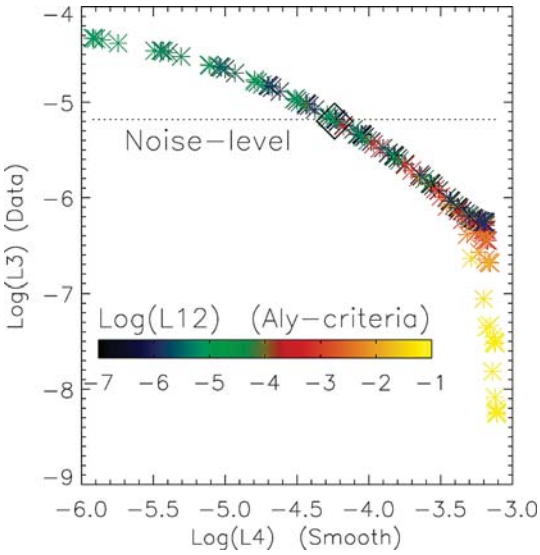

Figure 1. Survey of solutions to (8) in a phase space spanned by $\log(L_4)$ (abscissa), $\log(L_3)$ (ordinate), and $\log(L_{12})$ (color code). Every symbol corresponds to one solution $\mathbf{B}_{\min}$. The optimal parameters are marked with a rhombus. Here we have $L_{12} = 7.6 \times 10^{-7}$, $L_3 = 6.3 \times 10^{-6}$, and $L_4 = 5.8 \times 10^{-5}$. The optimal parameters are $\mu_3 = 0.01$ and $\mu_4 = 0.005$.

that the magnetic flux magnitudes and the corresponding magnetic field topology (which might become very complex for multiple magnetic sources, see Schrijver and Title, 2002) are not affected by the preprocessing.

4. Tests With the Low and Lou Solution

For a first test we use the semi-analytic solution found by Low and Lou (1990). This solution has been designed in particular to test nonlinear force-free extrapolation codes. The solution contains free parameters, and we use $\Phi = \pi/2$ and $l = 0.3$ (see Low and Lou (1990) for details). We extract the bottom boundary of this equilibrium and use it as input to our extrapolation code (see Wiegelmann (2004)). This artificial vector magnetogram (see first row of Figure 2) extrapolated from a semi-analytic solution is of course in perfect agreement with the assumption of a force-free field mentioned earlier (Aly criteria), and the result of our extrapolation code showed a reasonable agreement with the original. Real, measured, vector magnetograms are not so ideal (and smooth) of course and we simulate this effect by adding noise to the Low and Lou magnetogram. We add noise to this ideal solution in the form

Noise model I: $\delta B_i = n_l \, r_n \sqrt{B_i}$, where n_l is the noise level and r_n a random number in the range -1 to 1. The noise level was chosen to be $n_l = 5.0$ for

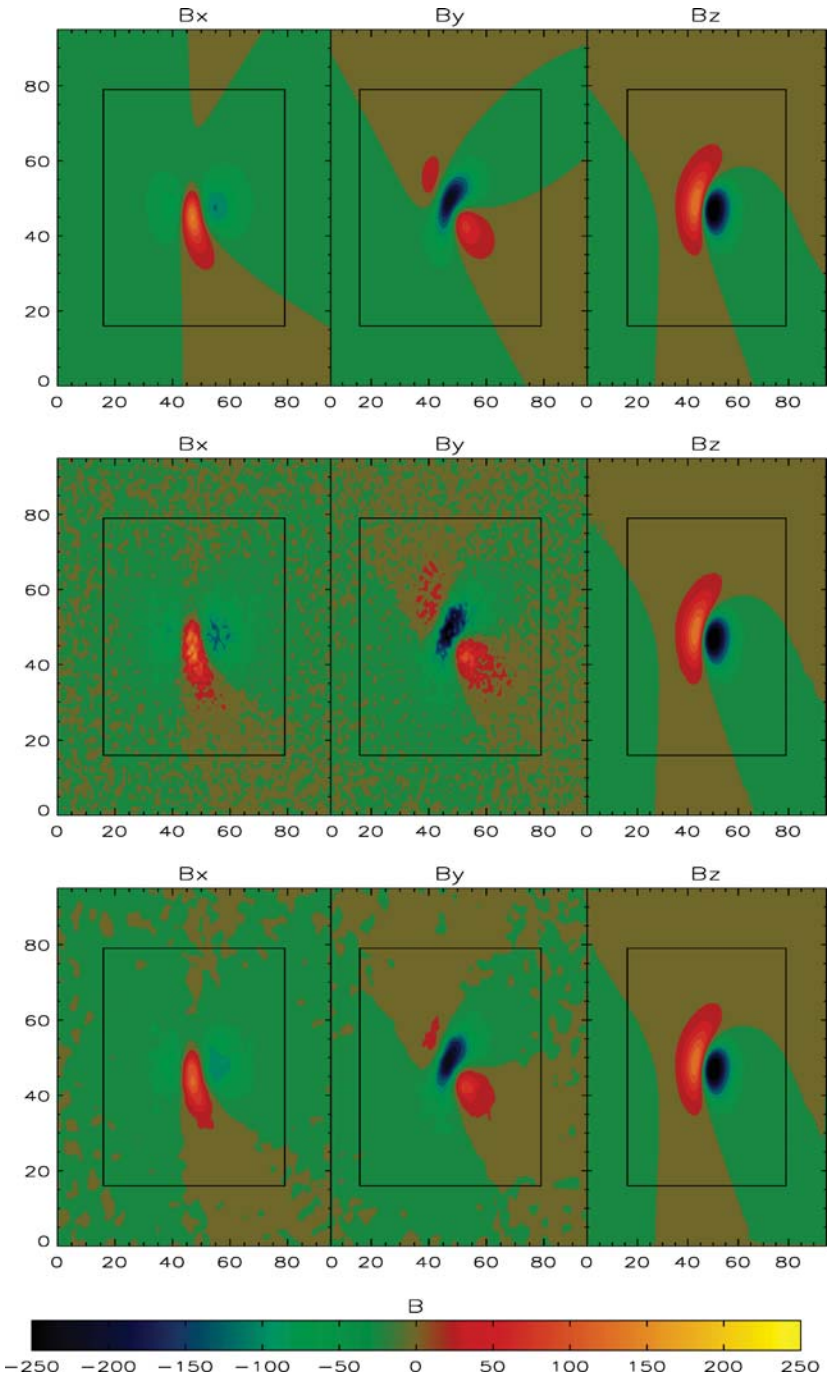

Figure 2. The first row shows the original vector magnetogram deduced from the Low and Lou solution. In the second row we added noise (model I) to the solution to simulate measurement errors. In the bottom row we applied our preprocessing routine to the noisy data taken from the center row.

the transverse magnetic field (B_x, B_y) and $n_l = 0.25$ for B_z. This mimics a real magnetogram (see center row of Figure 2) which has significantly higher noise in the transverse components of the magnetic field.

Noise model II: $\delta B_i = n_l\, r_n$, where n_l is the noise level and r_n a random number in the range -1 to 1. The noise level was chosen to be $n_l = 10.0$ for the transverse magnetic field (B_x, B_y) and $n_l = 0.5$ for B_z. This noise model adds an additive noise, independent from the magnetic field strength.

Noise model III: $\delta B_z = \text{constant}$, $\delta B_\text{t} = \delta B^2_\text{tmin} / \sqrt{B^2_\text{t} + \delta B^2_\text{tmin}}$ where we choose the constant noise level of B_z to be 1 and the minimum detection level $\delta B_\text{tmin} = 20$. This noise model mimics the effect that the transverse noise level is higher in regions with a low magnetic field strength, which is an immediate consequence of Equation (4).

The bottom row of Figure 2 shows the preprocessed vector magnetogram (for noise model I) after applying our procedure. The aim of the preprocessing is to use the resulting magnetogram as input for a nonlinear force-free magnetic field extrapolation. Figure 3 shows in panel (a) the original Low and Lou solution and in panel (b) a corresponding potential field reconstruction. In Figure 3 we present only the central region of the whole magnetogram (marked with black rectangular box in Figure 2 because the surrounding magnetogram is used as a boundary layer (16 grid points) for our nonlinear force-free code. (Our nonlinear force-free code is explained in detail in Wiegelmann (2004). The computation was done on a $96 \times 96 \times 80$ grid including a 16 pixel boundary layer adjacent to the lateral and top boundary of the computational box.) In the remaining panels of Figure 3 we demonstrate the effect of the different noise models on the reconstruction. The noise levels were chosen so that the mean noise was similar for all three noise models. Figure 3(c) shows a nonlinear force-free reconstruction with noisy data (noise model I, magnetogram shown in the center panel of Figures 2) and Figure 3(d) presents a nonlinear force-free reconstruction after preprocessing (magnetogram shown in the bottom panel of Figure 2). After preprocessing (Figure 3d) we get a much better agreement with the original solution (Figure 3a). Figure 3(e) and (f) show a nonlinear force-free reconstruction for noise model II without (e) and after (f) preprocessing of the noisy data. Figures 3(g) and (h) show a nonlinear force-free reconstruction for noise model III without (g) and after (h) preprocessing of the noisy data. As for noise model I, we find that the preprocessed data agree better with the original Figure 3(a). We check the correlation of the original solution with our reconstruction with the help of the vector correlation function VC defined as

$$VC = \frac{\sum_i \mathbf{v_i} \cdot \mathbf{w_i}}{\sqrt{\sum_i |\mathbf{v_i}|^2}\, \sqrt{\sum_i |\mathbf{w_i}|^2}}. \tag{14}$$

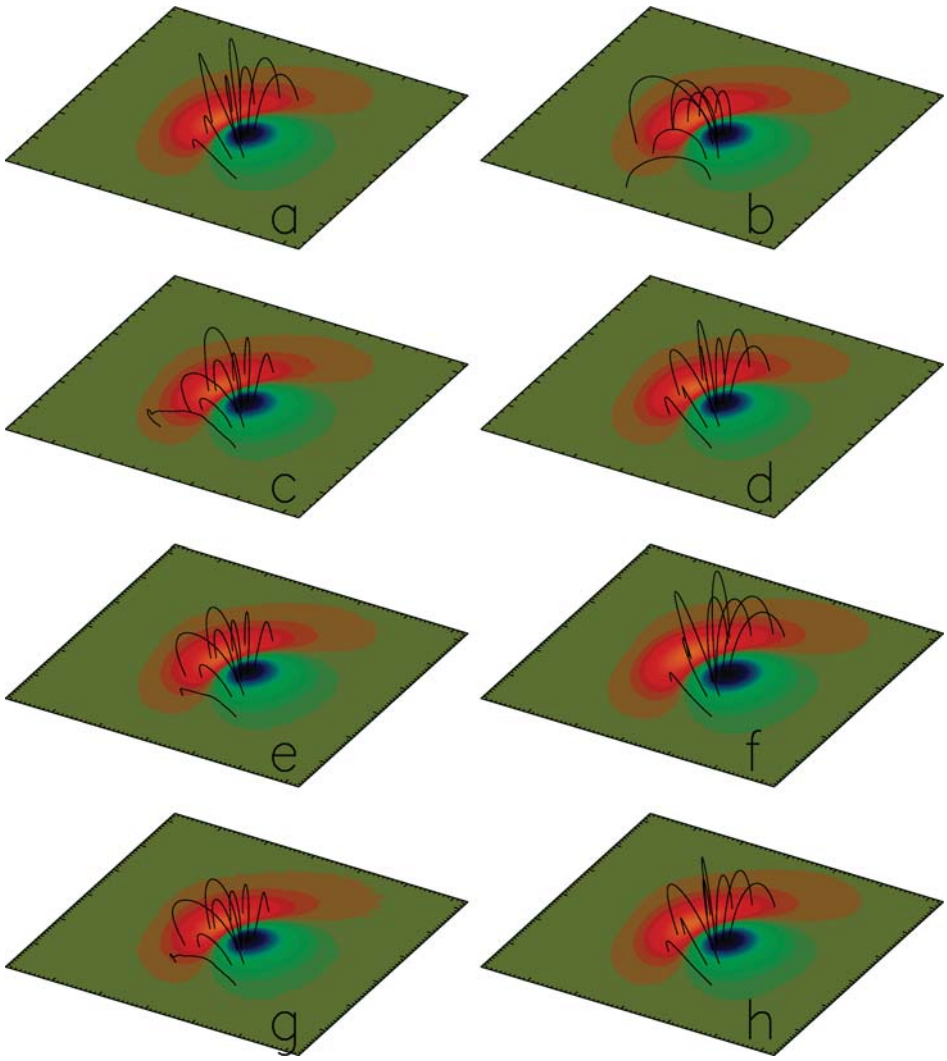

Figure 3. (a) Some field lines for the original Low and Lou solution. (b) Potential field reconstruction. (c) Nonlinear force-free reconstruction from noisy data (noise model I) without preprocessing. (d) Nonlinear force-free reconstruction from noisy data (noise model I) after preprocessing the vector magnetogram with our newly developed program. (e) Nonlinear force-free reconstruction from noisy data (noise model II) without preprocessing. (f) Nonlinear force-free reconstruction from noisy data (noise model II) after preprocessing. (g) Nonlinear force-free reconstruction from noisy data (noise model III) without preprocessing. (h) Nonlinear force-free reconstruction from noisy data (noise model III) after preprocessing the vector magnetogram with our newly developed program. The color coding shows the normal magnetic field component on the photosphere in all panel. One can see, that after preprocessing (panel d, f, h) the agreement with the original (a) is much better than without preprocessing (c, e, g).

where $\mathbf{v_i}$ corresponds to a reference field (Low and Lou solution) and $\mathbf{w_i}$ to the nonlinear force-free field reconstructed with our code.

Case	Remark	Preprocessing	Vector correlation
(a)	Reference		1.00
(b)	Potential		0.85
(c)	Noise model I	No	0.94
(d)	Noise model I	Yes	0.98
(e)	Noise model II	No	0.95
(f)	Noise model II	Yes	0.98
(g)	Noise model III	No	0.93
(h)	Noise model III	Yes	0.98

The table confirms the visual inspection of Figure 3. The correlation of the reconstructed magnetic field with the original becomes significantly improved after preprocessing of the data for all noise models. We knew already from previous studies (Wiegelmann and Neukirch, 2003; Wiegelmann, 2004) that noise and inconsistencies in vector magnetograms have negative influence on the nonlinear force-free reconstruction and the preprocessing routine described in this work tells us how to overcome these difficulties.

5. Application to Data from the Solar Flare Telescope (SFT)

In this section we apply our method to vector magnetogram data of AR 7321 taken with the SFT at the National Astronomical Observatory (NAO) in Tokyo. The SFT instrument is described by Sakurai *et al.* (1995) and the evolution of the photospheric magnetic field in AR 7321 has been studied by Li *et al.* (2000). The top panel of Figure 4 shows the original data (original resolution reduced by a factor of 2). and the bottom panel after preprocessing. The structure of all components of the magnetic field is similar to the original. The magnetogram is almost flux-balanced ($\epsilon_{\text{flux}} = 0.045$), but Aly's criteria are not fulfilled in the original ($\epsilon_{\text{Aly}} = 1.50$). After preprocessing, we get $\epsilon_{\text{Aly}} = 0.029$ and the data are also somewhat smoother than the original. The L-values of the original data and after preprocessing are:

		Original	Preprocessed
L_{12}	(Aly criteria)	0.58	3.6×10^{-5}
L_3	(data)	0.0	1.0×10^{-5}
L_4	(smoothing)	2.1×10^{-4}	5.2×10^{-6}

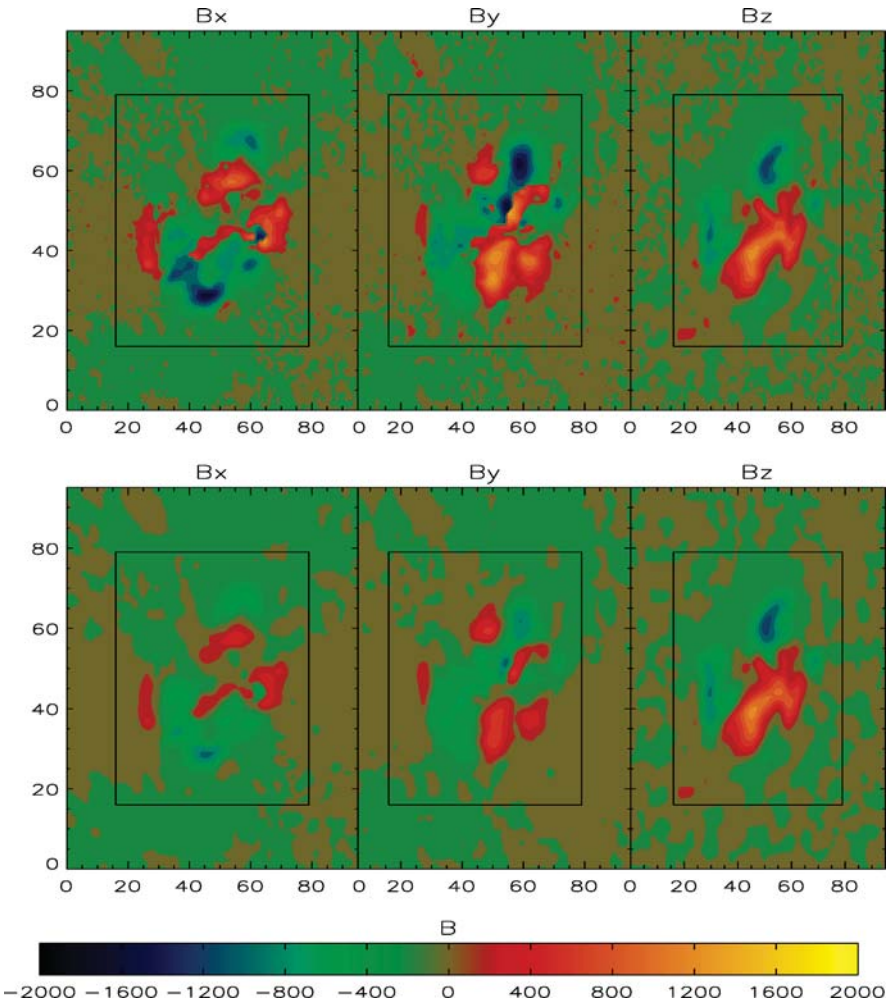

Figure 4. Top panel: Vector magnetogram of AR 7321 taken with SFT on October 26, 1992. *Bottom panel*: After applying our preprocessing procedure. The resolution of the original SFT magnetogram has been reduced by a factor of two to speed up the nonlinear force-free magnetic field reconstruction. An inspection of the top and bottom panels shows that local small scale structures with strong flux density in the original lead to a broader structure with weaker flux density after preprocessing. Sharp boundaries between positive and negative flux regions are also broadened due to smoothing during preprocessing.

Figure 5(a) shows a potential field reconstruction and Figure 5(b) a nonlinear force-free reconstruction based on the preprocessed vector magnetogram. The nonlinear force-free computation was done in a $96 \times 96 \times 80$ box, including a boundary layer of 16 grid points towards the lateral and top boundary. Figure 5 shows only the center cube of $64 \times 64 \times 64$ pixel which corresponds to the area marked with a black rectangular box in Figure 4.

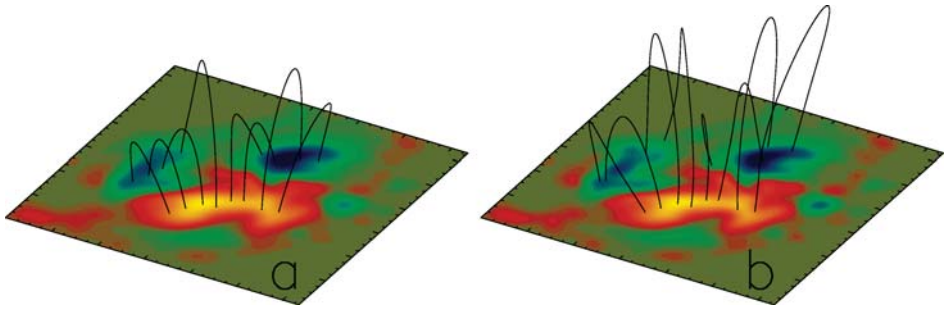

Figure 5. AR 7321 measured with SFT data from October 26, 1992. (a) Potential field reconstruction. (b) Nonlinear force-free reconstruction. The field lines start from the same footpoints within regions $B_z > 0$ in both panels.

6. Conclusions

Within this work we presented a method for the preprocessing of vector magnetogram data with the aim of using the result of the preprocessing as input for a nonlinear force-free magnetic field extrapolation with the help of an optimization code method. As a first test of the method, we use the Low and Lou solution with overlaid noise with different noise models. A direct use of the noisy photospheric data for a nonlinear force-free extrapolation showed poor agreement with the original Low and Lou solution, but after applying our newly developed preprocessing method we got a reasonable agreement with the original. The preprocessing method uses the high noise level in the transverse vector magnetogram components to drive the magnetogram towards boundary conditions which are consistent with the assumption of a force-free field mentioned earlier. To do so we use a minimization principle. On the one hand we require that the final boundary data are as close as possible (within the noise level) to the original measured data and on the other hand the data are forced to fulfill the Aly criteria and be sufficiently smooth. Smoothness of the boundary data is required for the nonlinear force-free extrapolation code, but also physically motivated because the magnetic field at the base of the corona should be smoother than in the photosphere, where it is measured.

Let us remark that nonlinear force-free extrapolations are only valid as long as the plasma β is low and nonmagnetic forces like pressure gradients and gravity can be neglected. This is usually the case in the corona (low-β plasma, $\beta \approx 10^{-4}$), but not in the photosphere ($\beta \approx 1$). A complete understanding of how the magnetic field evolves from the (non–force-free) photosphere through the chromosphere and transition region into the (force-free) corona would require more advanced models, at least magnetohydrostatic equilibria. Measurements of the photospheric magnetic field vector are not sufficient for such models and one needs additional observations regarding plasma quantities (*e.g.* density, temperature, pressure). A

magnetohydrostatic approach is also required to model prominences where the magnetic field counteracts the gravitational force of the material it supports.

We are applying our newly-developed preprocessing program to data taken with the Solar Flare Telescope and use the preprocessed boundary data for a nonlinear force-free field extrapolation.

Acknowledgements

The work of T. Wiegelmann was supported by DLR-grant 50 OC 0007 and a JSPS visitor grant at the National Astronomical Observatory in Tokyo. We thank the referee, Bruce Lites, for useful remarks.

References

Alissandrakis, C.E.: 1981, *Astron. Astrophys.* **100**, 197.
Aly, J.J.: 1989, *Solar Phys.* **120**, 19.
Amari, T., Aly, J.J., Luciani, J.F., Boulmezaoud, T.Z., and Mikic, Z.: 1997, *Solar Phys.* **174**, 129.
Arnaud, J. and Newkirk, G.: 1987, *Astron. Astrophys.* **178**, 263.
Chiu, Y.T. and Hilton, H.H.: 1977, *Astrophys. J.* **212**, 873.
Cuperman, S., Ofman, L., and Semel, M.: 1989, *Astron. Astrophys.* **216**, 265.
Demoulin, P. and Priest, E.R.: 1992, *Astron. Astrophys.* **258**, 535.
Gary, G.A.: 2001, *Solar Phys.* **203**, 71.
Hansen, P.C.: 2001, in P. Johnston (ed.), *Computational Inverse Problems in Electrocardiology*. WIT Press, Southampton, p. 19.
House, L.L.: 1977, *Astrophys. J.* **214**, 632.
Judge, P.G.: 1998, *Astrophys. J.* **500**, 1009.
Lagg, A., Woch, J., Krupp, N., and Solanki, S.K.: 2004, *Astron. Astrophys.* **414**, 1109.
Li, H., Sakurai, T., Ichimoto, K., and Ueno, S.: 2000, *Pub. Astron. Soc. Japan* **52**, 483.
Lin, H., Kuhn, J.R., and Coulter, R.: 2004, *Astrophys. J.* **613**, L177.
Low, B.C. and Lou, Y.Q.: 1990, *Astrophys. J.* **352**, 343.
Metcalf, T.R.: 1994, *Solar Phys.* **155**, 235.
Régnier, S., Amari, T., and Kersalé, E.: 2002, *Astron. Astrophys.* **392**, 1119.
Roumeliotis, G.: 1996, *Astrophys. J.* **473**, 1095.
Sakurai, T.: 1981, *Solar Phys.* **69**, 343.
Sakurai, T., Ichimoto, K., Nishino, Y., Shinoda, K., Noguchi, M., Hiei, E., Li, T., He, F., Mao, W., Lu, H., Ai, G., Zhao, Z., Kawakami, S., and Chae, J.: 1995, *Pub. Astron., Soc. Japan* **47**, 81.
Schmidt, H.U.: 1964, in W.N. Hess (ed.), *The Physics of Solar Flares*, NASA, Washington, DC, p. 107.
Schrijver, C.J. and Title, A.M.: 2002, *Solar Phys.* **207**, 223.
Seehafer, N.: 1978, *Solar Phys.* **58**, 215.
Seehafer, N.: 1982, *Solar Phys.* **81**, 69.
Semel, M.: 1967, *Ann. d'Astrophys.* **30**, 513.
Semel, M.: 1988, *Astron. Astrophys.* **198**, 293.
Solanki, S.K., Lagg, A., Woch, J., Krupp, N., and Collados, M.: 2003, *Nature* **425**, 692.
Valori, G., Kliem, B., and Keppens, R.: 2005, *Astron. Astrophys.* **433**, 335.

Wheatland, M.S.: 2004, *Solar Phys.* **222**, 247.
Wheatland, M.S., Sturrock, P.A., and Roumeliotis, G.: 2000, *Astrophys. J.* **540**, 1150.
Wiegelmann, T.: 2004, *Solar Phys.* **219**, 87.
Wiegelmann, T., Lagg, A., Solanki, S.K., Inhester, B., and Woch, J.: 2005, *Astron. Astrophys.* **433**, 701.
Wiegelmann, T. and Neukirch, T.: 2003, *Nonlinear Processes Geophys.* **10**, 313.
Wu, S.T., Sun, M.T., Chang, H.M., Hagyard, M.J., and Gary, G.A.: 1990, *Astrophys. J.* **362**, 698.
Yan, Y. and Sakurai, T.: 2000, *Solar Phys.* **195**, 89.